International Journal of Heat and Mass Transfer 102 (2016) 396–406

Contents lists available at ScienceDirect

International Journal of Heat and Mass Transfer

journal homepage: www.elsevier.com/locate/ijhmt

Measurement and simplified numerical prediction of effective thermal conductivity of open-cell ceramic foams at high temperature

Miguel A.A. Mendes [a,b,*], Pitt Goetze [a,*], Prabal Talukdar [c], Eric Werzner [a], Cornelius Demuth [a], Philip Rössger [a], Rhena Wulf [a], Ulrich Gross [a], Dimosthenis Trimis [a,b], Subhashis Ray [a,*]

[a] Institute of Thermal Engineering, Technische Universität Bergakademie Freiberg, Gustav-Zeuner-Strasse 7, D-09596 Freiberg, Germany
[b] Engler-Bunte-Institute Division of Combustion Technology, Karlsruhe Institute of Technology, Engler-Bunte-Ring 7, D-76131 Karlsruhe, Germany
[c] Department of Mechanical Engineering, Indian Institute of Technology Delhi, New Delhi 110016, India

ARTICLE INFO

Article history:
Received 18 February 2016
Received in revised form 3 May 2016
Accepted 8 June 2016
Available online 29 June 2016

Keywords:
Effective thermal conductivity
Oen-cell ceramic foams
Transient plane source technique
High temperature
1D conduction–radiation model
3D computed tomography

ABSTRACT

In the present article, the effective thermal conductivity (ETC) of 10 ppi open-cell ceramic foams is measured at temperatures ranging from 22 °C to 750 °C using the transient plane source (TPS) technique. The detailed morphology of the foam structures is reconstructed from 3D CT-scan images and their structural analysis is carried out using a volume image processing tool. The experimental results are compared with the predictions of directional ETC, obtained using a simplified 1D homogeneous model that considers coupled conduction–radiation heat transfer. The parameters, required by the model, are evaluated based only upon the information that could be extracted from 3D CT-scan images under certain simplifying assumptions. It can be concluded that the predictions of ETC for the present ceramic foam samples clearly correlate with the geometric parameters obtained from their structural analysis. It is also observed that the estimated microscopic porosity of the foam, which is not captured by 3D CT-scan images, has considerable influence on the reconstructed foam structure and hence on the predicted ETC. The predictions of ETC in the measured direction, obtained after the proposed directional averaging, compare extremely well with TPS measurements for the complete range of investigated temperatures. This suggests that the measurements of ETC, obtained employing TPS technique, are the directionally averaged representations of ETC in three perpendicular directions. The present investigation also clearly demonstrates the potential of the simplified modeling approach for characterizing even the directional ETC of open-cell ceramic foams, based primarily on their structural information.

1. Introduction

Ceramic porous foams exhibit several characteristics that promote their use in a wide variety of engineering applications. Among other characteristics, high thermal-shock, corrosion and abrasion resistance make these foams extremely suitable for high temperature systems, where they may be utilized for example, as: burner stabilizers [1–3], catalyst carriers [4], heat exchangers [5] or even metal melt filters [6]. In this context, the accurate evaluation of thermo-physical properties of the foam, particularly the effective thermal conductivity (ETC) at high temperatures, is important for a reliable prediction of the heat transfer behaviour and hence, for an appropriate design of the system.

Since the ceramic porous foams present a relatively high porosity, typically in the range from 70% to 90%, they often provide little contact area for the experimental determination of ETC. It is, therefore, hardly surprising that even though porous foams have been employed in a wide range of high temperature systems, there is no well established measurement technique in order to accurately determine their ETC, particularly at high temperatures.

The effective thermal conductivity of ceramic porous foams at high temperatures can be measured using either steady-state or transient methods. The steady-state methods available in the literature are generally based on either guarded hot-plate or panel test techniques. For example, Becker et al. [7] measured ETC of cordierite, clay-bound silicon carbide (CBSiC) and sintered silicon carbide (SSiC) foams in a temperature range from 80 °C to 500 °C, while Wang et al. [8] investigated the ETC of SiC and alumina foams in a temperature range from 80 °C to 300 °C. Dietrich et al. [9] measured ETC of alumina, Mullite and CBSiC foams, presenting various pore densities and porosities in the range from 75% to 85%. Their results were obtained for moderate temperatures up to 100 °C

* Corresponding authors at: Engler-Bunte-Institute Division of Combustion Technology, Karlsruhe Institute of Technology, Engler-Bunte-Ring 7, D-76131 Karlsruhe, Germany (M.A.A. Mendes).

E-mail addresses: miguel.mendes@kit.edu (M.A.A. Mendes), pitt.goetze@iwtt.tu-freiberg.de (P. Goetze), ray@iwtt.tu-freiberg.de (S. Ray).

http://dx.doi.org/10.1016/j.ijheatmasstransfer.2016.06.022
0017-9310/

Nomenclature

$\overline{D}_{por,str,win}$	overall mean diameter for pores, struts and windows, respectively, [m]
$\overline{D}_{x,y,z}$	mean pore diameter in x, y and z directions, respectively, [m]
$\dot{q}''$	steady-state heat flux [W/m^2]
$\hat{e}_x$	Cartesian unit vector for x coordinate
$\overline{S}_{spe}$	specific surface area [m^{-1}]
$\hat{s}$	direction vector for radiation intensity
b	adjustable parameter
I	radiation intensity [W/m^2 sr]
k	thermal conductivity [W/m K]
L	length, thickness [m]
s	distance along direction of radiation intensity [m]
T	temperature [K]
x	position coordinate [m]

Greek symbols

β	extinction coefficient [m^{-1}]
ε	emissivity
Θ	scattering angle
σ	Stefan–Boltzmann constant $= 5.67 \times 10^{-8}$ [W/m^2 K^4]
Φ	scattering phase function
ϕ_T	total porosity
ϕ_M	macroscopic porosity
ϕ_m	microscopic porosity
ρ	reflectivity
τ	transmissivity
Ω	solid angle [sr]
ω	scattering albedo

Subscript

av	average
B	bulk material
b	black body
C	conductive
c	cold
eff	effective
f	fluid
h	hot
max	maximum
min	minimum
R	radiative
r	representative
s	solid

Abbreviations

1D	one-dimensional
3D	three-dimensional
CT	Computed Tomography
ETC	effective thermal conductivity
FVM	finite volume method
ppi	pores-per-inch
RTE	radiative transfer equation
TPS	transient plane source

using a guarded hot-plate apparatus in combination with a numerical procedure in order to correct the heat losses. Very recently, Dietrich et al. [10] and Fischedick et al. [11] reported an extended version of their previous investigation [9], where ETC of ceramic foams was measured up to 1000 °C by applying a guarded hot-plate apparatus combined with a finite difference method for solving the energy balance considering both conduction and radiation based on the homogenization approach.

As far as the transient methods for measuring ETC of ceramic porous foams are concerned at high temperatures, Liaw et al. [12], Skidan et al. [13] and Lo et al. [14] applied the transient hot-wire technique up to 1000 °C in order to investigate ETC of alumina foams prepared by direct foaming and therefore, presenting small mean pore diameters. Coquard et al. [15] predicted ETC of open-cell mullite and zirconia foams by introducing the experimentally acquired temperature field into their numerical model for heat transfer. The referred temperature field was obtained from the thermal response of the foam samples to a laser impulse, which was recorded over time using an infrared camera.

In order to control ETC of foams, a deeper understanding of the influence of the foam structure on its heat transfer characteristics is necessary. Due to the coupled nature of conduction and radiation heat transfer at high temperatures and since the ceramic porous foams are most often characterized by complex structures, they are difficult to access by the conventional measurement techniques. Particularly, it is considerably difficult to determine the details of individual contributions of both conduction and radiation [16]. In this respect, the numerical heat transfer models, that are based on the detailed information of the foam structure, provide a promising complement or even a better alternative for the investigation of ETC of porous foams, particularly at high temperatures. Reviews on the existing models for predicting ETC of porous foams at both ambient and higher temperatures are provided by Coquard and Baillis [17] and Coquard et al. [18].

Several researchers [18–21] attempted to synthetically generate equivalent regular structures (e.g., cubic or Kelvin cells) that can only approximate the real foams for the purpose of estimating ETC to some extent, since most of the intricate structural details are lost during such idealizations. In this respect, recently more sophisticated methods (e.g. Laguerre tessellation coupled with implicit functions [22] or 3D Voronoi methods [23]) have been developed in order to generate more realistic open-cell foams, presenting an irregular structure. Alternatively, three-dimensional (3D) Computed Tomography (CT)-scan imaging technology allows one to employ the true morphology of porous foams in the numerical heat transfer models for predicting ETC, although the computational cost of these simulations most often increases significantly depending upon the required spatial resolution of CT and the size of the representative foam sample. Effective properties of porous foams for both conduction [21,24,25] and radiation [26–28] have been numerically evaluated in several recent investigations, using the nearly exact geometry of the foam sample obtained from 3D CT-scan data.

Recently, Mendes et al. [29] have numerically evaluated ETC at high temperatures by solving the coupled conduction–radiation heat transfer problem for open-cell porous foams, while considering both detailed 3D and simplified 1D modeling approaches, where the complex structures of the foams were obtained from high resolution 3D CT-scan images. They have concluded that the detailed 3D modeling approach, which is based on the method proposed by Talukdar et al. [20], is accurate yet computationally prohibitive for evaluating ETC of large foam samples. On the other hand, they have pointed out that the alternative simplified 1D modeling approach, which is based on the assumption of homogenization and superposition of conduction and radiation, is computationally more efficient than the detailed approach and yielded reasonably accurate results for ETC, since the required model parameters in this method are estimated based on 3D CT-scan

data. In a subsequent study [30], the performance of this simplified 1D homogeneous model was examined by comparing the predictions with measurements of ETC of open-cell metal foams at high temperatures, ranging from 130 °C to 850 °C. The results, presented by Mendes et al. [30], clearly demonstrate that the simplified model performs extremely well at both ambient and higher temperatures. This observation may be partially attributed to the reasonably accurate estimation of the major model parameters (i.e. ETC due to pure heat conduction and the extinction coefficient) using simple numerical tools while relying only upon the information extracted from 3D CT-scan images.

The primary objective of the present investigation is to predict ETC of open-cell ceramic foams at higher temperatures employing the simplified 1D homogeneous model of Mendes et al. [29,30] and to compare the resulting predictions with the respective measurements obtained using the transient plane source (TPS) technique. For the simplified 1D homogeneous model, the structure of the ceramic foam is obtained from the high resolution 3D CT-scan images. This data also allows for an analysis of the foam structure that can be further related to the results of ETC, with respect to both anisotropy and microscopic porosity of foams. Therefore, the results obtained during the present investigation validate and demonstrate the potential of the considered modeling approach for characterizing ETC of open-cell ceramic foams, based primarily on their structural information.

2. Experimental investigation

Two large samples of open-cell porous foams, made of pure alumina with a pore density of 10 ppi (referred to as Sample-1 and Sample-2), are considered for the present study. These foams contain a similar total porosity $\phi_T = 0.89$ that is determined by gravimetric weighing and measuring the dimensions (60 mm × 120 mm × 120 mm) of the samples, while considering the density of pure alumina to be 3984 kg/m^3 [31]. The structural details of these foam samples are obtained from 3D CT-scan images with a resolution of 70 μm, as presented in Fig. 1(a) for Sample-1. Based on this information and subsequently using a volume image processing tool, several structural parameters of the foam samples are evaluated, e.g. the specific surface area $\overline{S}_{spe}$, the overall mean diameter for struts $\overline{D}_{str}$, windows $\overline{D}_{win}$ and pores $\overline{D}_{por}$, as well as the mean pore diameters in x, y and z directions $\overline{D}_{x,y,z}$ (see [32] for details). For better clarity, Fig. 1(b) shows a region of the 10 ppi alumina foam, including the definitions of overall mean diameter for struts, windows and pores. The evaluated structural parameters are provided in Table 1, where the variation in $\overline{D}_{x,y,z}$ clearly confirms that the shape of the pores is ellipsoidal instead of being spherical. Therefore, it can be legitimately concluded that the foam samples are truly anisotropic. This anisotropy is expected to have a corresponding relevant influence on ETC of these foams, as will be discussed in Section 4.

The effective thermal conductivity of the alumina foam samples is measured using TPS technique proposed by Gustafsson [33]. The TPS apparatus, considered for the present investigation was employed previously in another investigation reported by Wulf [34] for measuring ETC of metal foams at ambient temperature. Although the TPS technique, applied to opaque materials without radiation, is quite well established for measuring the purely conductive heat transfer, some questions may arise about the accuracy of this technique for measuring the thermal conductivity of semi-transparent materials with significant radiation contribution, e.g. porous foams or low-density thermal insulators. Nevertheless, Coquard et al. [35] investigated the accuracy of the TPS technique for measuring the thermal conductivity of semi-transparent materials and demonstrated that the presence of a radiative contribution does not affect the accuracy of the measurement since the measured thermal conductivity accounts for both conduction and radiation contributions.

Hot disk 的缺陷

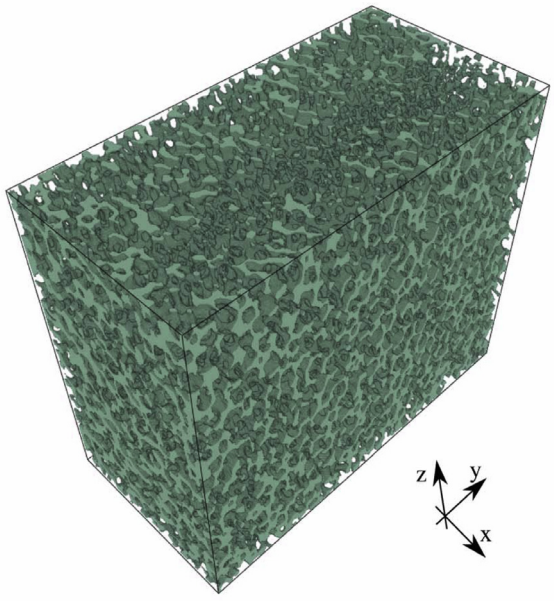

(a)

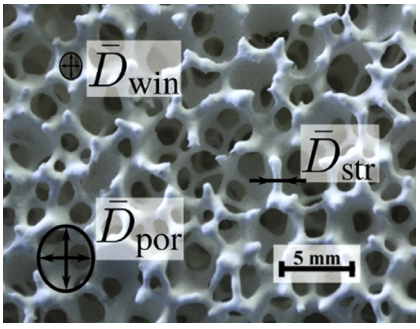

(b)

Fig. 1. 10 ppi alumina foam (Sample-1): (a) structure obtained from 3D CT-scan images; (b) definitions of overall mean diameter for struts, windows and pores.

表明材料是各向异性

Table 1
Geometric parameters obtained from structural analysis using image processing tool for 10 ppi foam samples (x, y and z directions are shown in Figs. 1(a) and 2).

Parameter	Sample-1	Sample-2
$\overline{S}_{spe}$ [m^{-1}]	643	649
$\overline{D}_{str}$ [mm]	0.7	0.7
$\overline{D}_{win}$ [mm]	3.3	3.2
$\overline{D}_{por}$ [mm]	4.8	4.7
$\overline{D}_{x}$ [mm]	5.4	5.2
$\overline{D}_{y}$ [mm]	4.3	4.1
$\overline{D}_{z}$ [mm]	4.2	4.1

The measurement principle of the TPS method is briefly presented here for the sake of completeness. In this method, an insulated sensor is placed between two identical parallelepipedic foam samples that simultaneously serves as heat source and resistance thermometer, as shown in Fig. 2. After applying a constant current to the heating element of the sensor, a transient, ellipsoidal temperature field developes. By correlating the resulting time evolu-

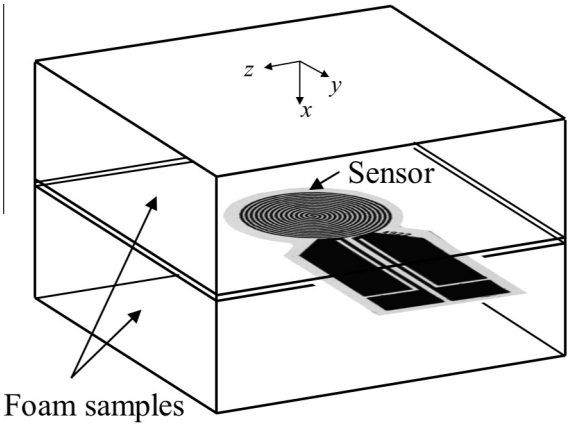

Fig. 2. Schematic representation of foam samples and sensor assembly for transient plane source technique.

tion of the temperature with the thermo-physical properties of the foam samples, ETC is determined (refer to Wulf et al. [34] for details).

Two types of sensors are employed for the present measurements of ETC. They are Kapton and Mica insulated sensors with a diameter of 14.9 mm (Hot Disk model 4922L) that cover temperatures below 300 °C and above 250 °C, respectively. Before, the sensor is sandwiched between the two foam samples, their surfaces are polished in order to improve the contact between sample and sensor. The setup is placed inside a protective gas chamber of a CWF 11/23/ E2416CG furnace (manufactured by Carbolite). The presence of protective gas atmosphere, consisting of nitrogen, is extremely important in order to avoid oxidation of the Mica sensor at temperatures above 400 °C. For avoiding the penetration of oxygen into the furnace chamber, a constant gauge pressure of 2 kPa for nitrogen is always ensured.

After determining the optimal heating power and measurement duration for the present sensors (see Bohac et al. [36]) and considering the heat penetration depth provided by the sensor manufacturer, ETCs of two foam samples are measured at different temperatures ranging from 22 °C to 750 °C. The uncertainties in the measurements of ETC estimated by the manufacturer are smaller than 5% and the reproducibility of the experimental results is found to lie within ±2% around the mean. It may be mentioned here that the measurements of ETC are repeated several times for the entire temperature range, while keeping the sensor positioned at the geometric center of the surfaces between two foam samples. However, the measurements are avoided at the intermediate temperatures, ranging from 300 °C to 400 °C. This is due to the fact that the metallic element of the sensor, which acts simultaneously as a resistance thermometer as well as a heat source, is made of nickel and has a Curie point of approximately 360 °C. Therefore, the electrical resistance of nickel changes strongly with temperature close to this point and hence the measurements are not recommended under this condition in order to avoid erroneous experimental results.

居里点

3. Modeling approach

The effective thermal conductivities of open-cell porous foams at high temperatures are also numerically predicted based on the detailed foam structure, which is obtained from the high resolution 3D CT-scan images. The foam is assumed to be composed of two distinct phases: a solid and a fluid phase, with thermal conductivities k_s and k_f, respectively. In addition, the fluid phase is assumed to be transparent as far as the radiation heat transfer is concerned. For the present investigation, the considered representative size of the foam samples is significantly large, as explained in Section 2, and since the CT resolution is 70 μm, which is also relatively high, a detailed 3D simulation for the coupled conduction–radiation heat transfer, similar to that proposed by Talukdar et al. [20], is computationally prohibitive. Therefore, a considerably simplified modeling approach, originally proposed and validated by Mendes et al. [29,30], is employed for the present study which is briefly described here for the sake of completeness.

For a representative sample of an open-cell porous foam, as schematically shown in Fig. 3, ETCs at different temperatures in a particular direction, say for example x, are numerically predicted from the converged temperature solutions based on the averaged Fourier's law of heat conduction:

$$k_{\text{eff}} = \frac{\dot{q}''_{\text{av}} L_{\text{r}}}{(T_{\text{h}} - T_{\text{c}})} \tag{1}$$

where $\dot{q}''_{\text{av}}$ and L_{r} are the average steady-state heat flux in the x-direction and the representative size of sample, respectively, while a temperature difference $T_{\text{h}} - T_{\text{c}}$, with $T_{\text{h}} > T_{\text{c}}$, is applied between the boundaries of the computational domain in x-direction. The remaining four boundaries (refer to Fig. 3) are assumed to be adiabatic in order to ensure one-directional heat transfer in an averaged sense. While $L_{\text{r}}, T_{\text{h}}$ and T_{c} are either known or prescribed parameters, $\dot{q}''_{\text{av}}$ has to be determined numerically in order to evaluate k_{eff} from Eq. (1).

3.1. Simplified 1D homogeneous model

Based on the investigations of Mendes et al. [29,30], a simplified 1D homogeneous model is employed for the numerical evaluation of $\dot{q}''_{\text{av}}$. This model, other than relying upon the homogenization approach, considers the coupled conduction–radiation problem in a 1D framework. Most importantly, it provides a more efficient yet considerably accurate alternative to the detailed 3D simulations for estimating ETC of open-cell porous foams at higher temperatures, where the radiation heat transfer plays an extremely important role.

For the simplified 1D model, the following steady-state energy conservation equation for coupled conduction–radiation heat transfer is solved [29,30]:

$$\frac{d}{dx}\left(k_{\text{eff,C}} \frac{dT}{dx}\right) - \frac{d\dot{q}''_{\text{R}}}{dx} = 0 \tag{2}$$

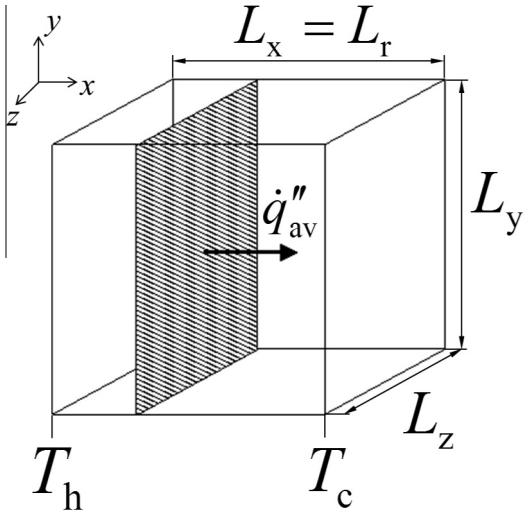

Fig. 3. Representative computational domain used for the numerical calculation of ETC with $L_x = 60$ mm, $L_y = L_z = 120$ mm.

where T and $k_{eff,C}$ are the local temperature and ETC due to the pure heat conduction, respectively. The gradient of radiative heat flux $d\dot{q}''_R/dx$ in Eq. (2) is considered as the source term. Eq. (2) is discretized and solved using the Finite Volume Method (FVM) [37], where the calculation of $d\dot{q}''_R/dx$ is accomplished from the solution of the Radiative Transfer Equation (RTE) for a gray, absorbing, emitting and scattering medium. The 1D RTE is given as [38]:

$$\frac{1}{\beta}\frac{dI(x,\hat{s})}{ds} = -I(x,\hat{s}) + (1-\omega)I_b(x) + \frac{\omega}{4\pi}\int_{4\pi} I(x,\hat{s}_i)\Phi(\hat{s}_i,\hat{s})d\Omega_i \quad (3)$$

where the unit vector $\hat{s}$ describes the direction of radiative intensity I and β is the extinction coefficient for radiation. Moreover, ω and Φ are the scattering albedo and scattering phase function of the medium, respectively, and $I_b = \sigma T^4/\pi$ is the intensity of black body radiation, where σ is the Stefan–Boltzmann constant.

Based on the distribution of radiation intensity, obtained from the solution of Eq. (3), $d\dot{q}''_R/dx$ in Eq. (2) can be evaluated as:

$$\frac{d\dot{q}''_R}{dx} = \beta(1-\omega)\left(4\pi I_b - \int_{4\pi} I(x,\hat{s})d\Omega\right) \quad (4)$$

The RTE is numerically solved using the discrete transfer method [39–41], where the details of the overall numerical procedure for solving Eqs. (2)–(4) were reported by Mishra et al. [42]. Finally, from the converged solution of the coupled conduction–radiation problem, $\dot{q}''_{av}$ can be obtained by post-processing as:

$$\dot{q}''_{av} = -k_{eff,C}\frac{dT}{dx} + \int_{4\pi} I(x,\hat{s})(\hat{s}\cdot\hat{e}_x)d\Omega = \text{constant}, \forall_x \quad (5)$$

Therefore, ETC of porous foams due to combined conduction and radiation can be calculated according to Eq. (1).

3.2. Evaluation of model parameters

The important parameters, required for the simplified 1D homogeneous model, described in the foregoing text, are $k_{eff,C}$ (for pure conduction) as well as β, ω and Φ (for radiation). In a manner, similar to that adopted by Mendes et al. [30], $k_{eff,C}$ and β are evaluated based only upon the information that could be extracted from 3D CT-scan images under certain simplifying assumptions, as will be shortly apparent. On the other hand, ω and Φ are estimated based on some approximations, which do not require any information from the 3D CT-scan images.

The evaluation of $k_{eff,C}$ based on the detailed 3D simulation of pure heat conduction problem, while accounting for the presence of both solid and fluid phases, requires considerably less computational time (about three orders of magnitude faster) as compared to that for the combined conduction–radiation problem in 3D [29]. Nevertheless, this detailed solution is still computationally very expensive owing to the large dimensions of foam samples considered for the present study. Therefore, the simplified approach proposed by Mendes et al. [21] is used for evaluating $k_{eff,C}$, where the heat conduction only through the solid medium is solved and hence the computational effort of the method is significantly reduced, while sacrificing a certain amount of accuracy. The validity of this approach was already demonstrated by Goetze et al. [32], where is was observed that for the present 10 ppi foam samples, the simplified model always yields relative errors lower than 1.5% for $k_{eff,C}$. In this method, $k_{eff,C}$ is estimated as [21]:

$$k_{eff,C} = bk_{min} + (1-b)k_{max} \quad (6)$$

where k_{min} and k_{max} are the minimum and the maximum possible values for $k_{eff,C}$, respectively, that are obtained according to the Hashin–Shtrikman bounds [43] and b is an adjustable parameter [21] specific for a given foam.

$$k_{min} = k_f\left[\frac{2k_f + k_s - 2(k_f - k_s)(1-\phi_M)}{2k_f + k_s + (k_f - k_s)(1-\phi_M)}\right] \quad (7a)$$

$$k_{max} = k_s\left[\frac{2k_s + k_f - 2(k_s - k_f)\phi_M}{2k_s + k_f + (k_s - k_f)\phi_M}\right] \quad (7b)$$

$$b = 1 - \frac{(2+\phi_M)}{2(1-\phi_M)}\frac{k_{eff,s}}{k_s} \quad (7c)$$

It is evident from Eq. (7) that the evaluation of k_{min} and k_{max} requires information about the thermal conductivities of the fluid and the solid phases, i.e. k_f and k_s, respectively, as well as the macroscopic porosity of the foam ϕ_M, which can be adequately captured by the present CT voxel resolution of 70 μm. The adopted procedures for estimating k_f, k_s and ϕ_M are discussed in detail in Section 3.3. Additionally, evaluation of b from Eq. (7c) also requires the dimensionless ETC of the foam under vacuum condition $k_{eff,s}/k_s$. This is determined from a single numerical prediction of ETC using the detailed 3D foam geometry, but only due to the presence of solid matrix by completely disregarding the contribution of heat conduction through the fluid phase since $k_f = 0$ [21]. Owing to the definition of $k_{eff,s}/k_s$, its evaluation is even independent of k_s and requires significantly reduced computational time, which scales at least to the order of ϕ_M [21,32]. It was already explained by Mendes et al. [21] that $k_{eff,s}/k_s$ is a characteristic property of the open-cell porous foams.

The extinction coefficient β is estimated using the image superposition technique, proposed by Loretz et al. [27] for metallic foams, which is also based on the detailed foam structure obtained from 3D CT-scan images. In this method, β in a particular direction is calculated from Beer's law as:

$$\beta = -\frac{\log(\tau)}{L} \quad (8)$$

where the transmissivity τ of the foam structure is obtained as the ratio of cross-sectional area covered by the fluid pixels to the total cross-sectional area of the sample, perpendicular to the direction of calculation, and L is the thickness of the foam considered for the image superposition. Although this method may be regarded quite accurate if its simplicity is taken into account, it tends to underes-

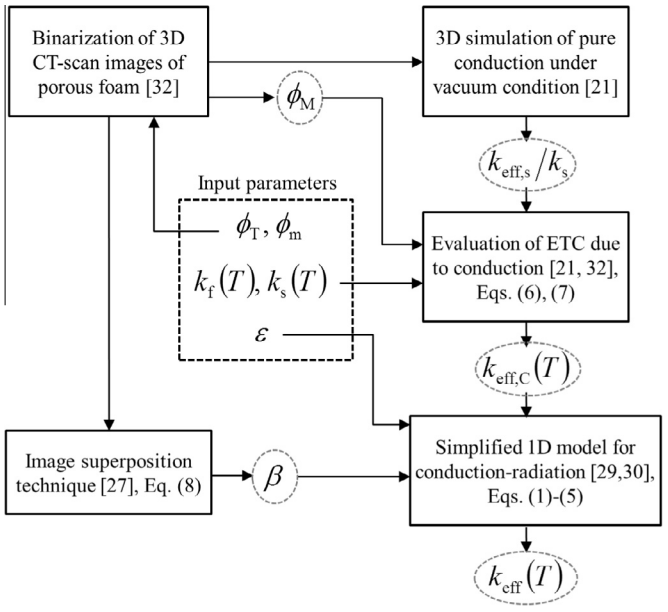

Fig. 4. Methodology for evaluating ETC of open-cell porous foams using the simplified 1D modeling approach.

timate β as compared to its measured value [23,27]. Further details of the method may be found in earlier articles [29,30], although some additional information is provided in Section 4.

The scattering albedo ω is taken equal to the reflectivity ρ of the foam surface [18,30], based on the assumption that the solid surface of the present ceramic foam samples is diffuse, opaque and gray. This assumption is quite reasonable since for the temperature range investigated in the present study (22–750 °C), the alumina structure of the foam has a nearly opaque surface, presenting a microscopic roughness that promotes diffuse reflection and emission of thermal radiation independent of its wavelength [44]. Therefore, $\omega = \rho = 1 - \varepsilon$ is obtained as a consequence of Kirchhoff's law for opaque surfaces, i.e. $\rho + \varepsilon = 1$, and hence ω can be directly evaluated provided the emissivity ε of the foam surface is known.

The scattering phase function Φ is approximated as that for large diffuse gray spheres [28], which can be expressed in terms of scattering angle Θ as [38]:

$$\Phi(\Theta) = \frac{8}{3\pi}(\sin\Theta - \Theta\cos\Theta) \tag{9}$$

In summary, it may be mentioned that the simplified 1D homogeneous model, described here, essentially requires three input parameters, namely $k_{\mathrm{eff,C}}$, β and ε, that depend on the foam structure as well as on the properties of constituent phases of the foam, as explained in the following.

3.3. Methodology for simplified 1D modeling approach

Fig. 4 provides an overview of the complete methodology, followed in the present study in order to evaluate k_{eff} based on the simplified 1D modeling approach. To start with, the 3D CT-scan data is obtained in the form of gray scale images that are then binarized into fluid (black) and solid (white) voxels by fixing the threshold gray color, as explained in the following. At first, ϕ_{M} is evaluated in the present study as [32]:

$$\phi_{\mathrm{M}} = \frac{\phi_{\mathrm{T}} - \phi_{\mathrm{m}}}{1 - \phi_{\mathrm{m}}} \tag{10}$$

where the total porosity of the foam ϕ_{T} can be easily and accurately determined experimentally, as described in Section 2. On the other hand, ϕ_{m} is the microscopic porosity within the bulk solid material, which depends strongly on the manufacturing process and hence only a rough estimation can most often be obtained [32]. Although some of the micro-pores could be resolved up to certain extent using much higher resolution CT-scan images, this is not performed during the present investigation due to limitations of the available CT technique. Quite evidently, depending upon the estimated value

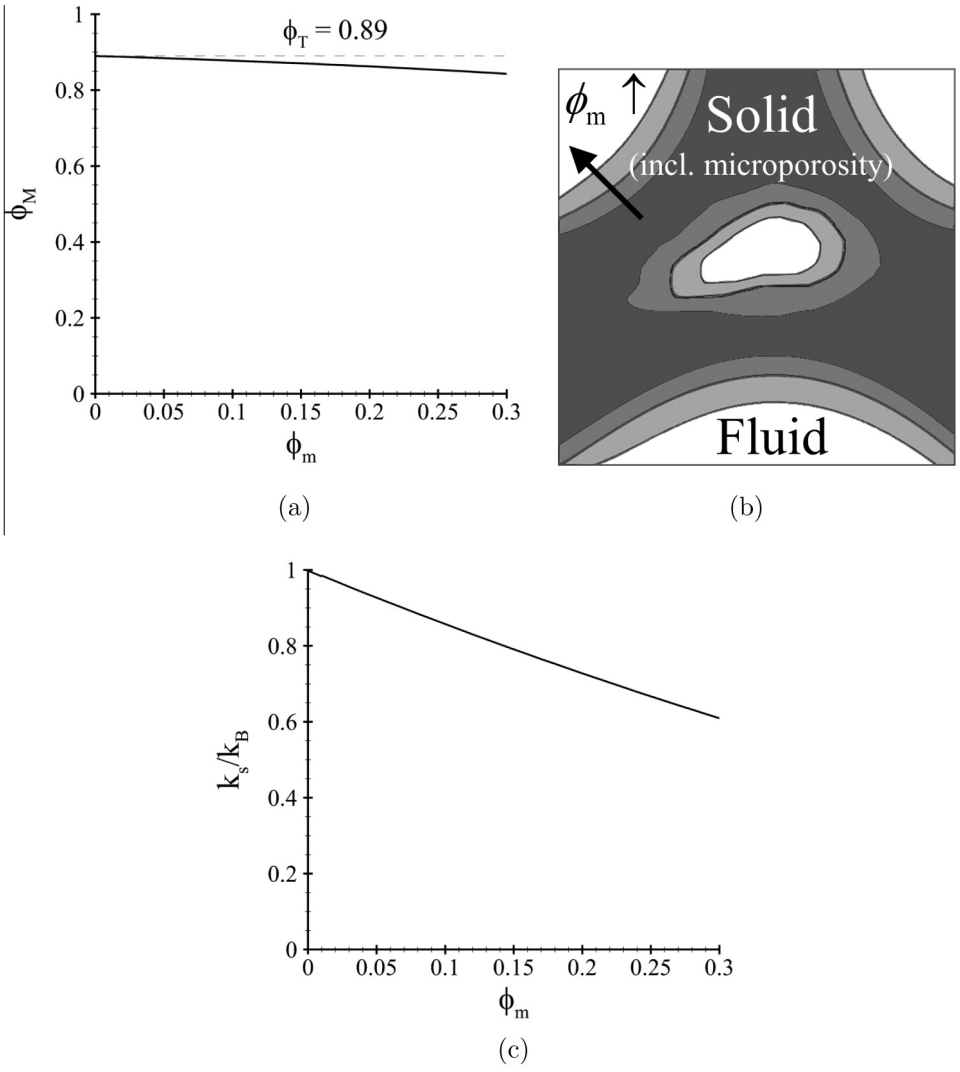

Fig. 5. Influence of ϕ_{m} on different foam characteristics during binarization of the 3D CT-scan images: (a) macroscopic porosity; (b) foam structure; (c) thermal conductivity ratio of equivalent solid phase to bulk solid material.

of ϕ_m, ϕ_M changes according to Eq. (10), as shown in Fig. 5(a). Similar effects may be observed on the predicted values of ETC.

The value of ϕ_M, calculated from ϕ_T and ϕ_m using Eq. (10), is used in order to fix the threshold gray color for the binarization of 3D CT-scan images of the porous foam into fluid and solid voxels. As a result, the foam structure is affected depending upon ϕ_m, as schematically shown in Fig. 5(b).

The binarized 3D structure of the porous foam, as shown in Fig. 1(a), is then used as an input for estimating β and calculating $k_{eff,s}/k_s$. It is important to note that both β and $k_{eff,s}/k_s$ are considered to be parameters that depend solely on the structure of the foam and are independent of the material properties, which is an approximation for the case of β.

Subsequently, $k_{eff,C}$ is evaluated on the basis of $k_{eff,s}/k_s, k_f$ and k_s, considering the last two parameters as functions of the foam temperature. While the thermal conductivity of the fluid phase k_f can most often be obtained from the literature, the thermal conductivity of the equivalent (or 'idealized') solid phase k_s depends on the aforementioned microscopic porosity, which could not be captured by the present CT-scan images. Therefore, k_s is expected to be smaller than the thermal conductivity of the bulk (or 'real') solid material k_B and is modeled for the present investigation using the upper Hashin–Shtrikman bound, analogous to Eq. (7b), which is given as [32]:

$$k_s = k_B\left[\frac{2k_B + k_f - 2\phi_m(k_B - k_f)}{2k_B + k_f + \phi_m(k_B - k_f)}\right] \tag{11}$$

where k_f, k_B and ϕ_m are considered as inputs. The variation of k_s/k_B as a function of ϕ_m for $T = 20\,°C$ (room temperature) according to Eq. (11) is presented in Fig. 5(c) as a demonstration, considering $k_f = 0.026$ W/mK and $k_B = 32.62$ W/mK.

Finally, k_{eff} is evaluated from the simplified 1D homogeneous model, based on the previously calculated β and $k_{eff,C}$ as well as ε, either obtained or estimated from some available source.

4. Results and discussions

The effective thermal conductivities of two 10 ppi pure alumina foam samples (see Table 1) are measured at temperatures ranging from 22 °C to 750 °C using TPS technique as explained in Section 2. Additionally, ETCs in the similar range of temperature are predicted employing the simplified 1D homogeneous model, as described in Section 3, and the predictions are compared with the measurements. The predicted results for ETC, as well as the related model parameters, are finally presented as the average of the individual values obtained for both samples (Sample-1 and Sample-2), since the experimental results are obtained in the same manner owing to the measuring principle of TPS technique, as explained in Section 2. However, it is also observed that the predictions, obtained from the model, are quite similar to each other for both foam samples since they have nearly identical structural parameters, as presented in Table 1.

For the numerical predictions, nitrogen is considered as the fluid phase since the same gaseous atmosphere is used for the measurements, whereas the microscopic pores within the modeled solid phase, that are formed during manufacturing, are assumed to be filled up by air. The latter assumption is invoked as there is no clear information available on the gas composition inside of the

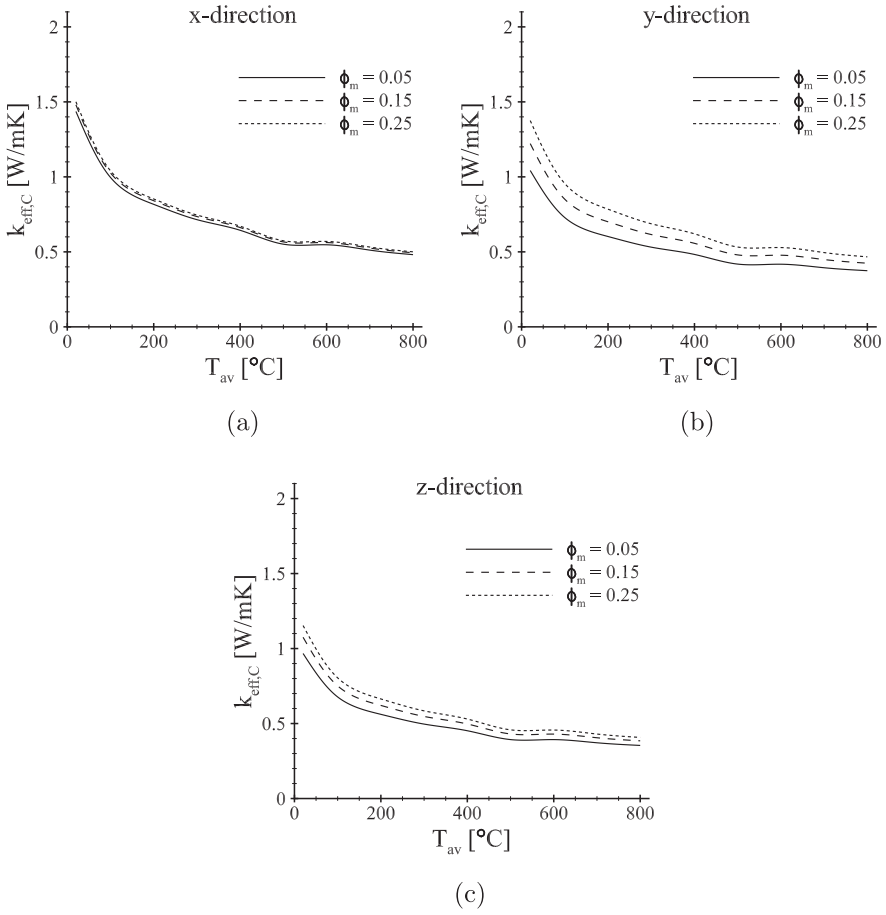

Fig. 6. Predicted ETC due to pure heat conduction in different directions as function of the average temperature for different ϕ_m: (a) *x*-direction; (b) *y*-direction; (c) *z*-direction.

micro-pores present in the solid phase, which is particularly true for the closed micro-pores that may contain gaseous species formed during the pyrolysis of the polyurethane foam, used as the template for producing the ceramic foam. Therefore, k_s is evaluated according to Eq. (11), considering k_B for pure alumina and k_f for air as functions of temperature in the form of available correlations [31,45]:

$$k_B(T) = 35.818 - 0.171T + 5.7\times10^{-4}T^2 - 1.0\times10^{-6}T^3 + 9.8\times10^{-10}T^4 - 4.7\times10^{-13}T^5 - 8.8\times10^{-17}T^6,\ (20^\circ\mathrm{C} \leqslant \mathrm{T} \leqslant 1500^\circ\mathrm{C}) \quad (12a)$$

$$k_f(T) = 2.4098\times10^{-2} + 7.8719\times10^{-5}T - 3.6119\times10^{-8}T^2 + 1.5207\times10^{-11}T^3,\ (20\ ^\circ\mathrm{C} \leqslant T \leqslant 1500\ ^\circ\mathrm{C}) \quad (12b)$$

where T is in °C and thermal conductivities are in W/mK. Since the thermal conductivity of nitrogen is almost identical to that of air (both may be considered as diatomic ideal gases) in the considered range of temperature, k_f for the fluid in the macro-pores is also evaluated according to Eq. (12b). Additionally, the emissivity of the pure alumina foam surface, required for the simplified 1D modeling approach, is considered as a function of temperature according to [46]:

$$\varepsilon(T) = 0.932 - 3.9\times10^{-4}T \quad (13)$$

where T is also in °C.

The microscopic porosity ϕ_m within the modeled solid phase, which is required in Eqs. (10) and (11), is expected to be approximately 0.15 for the present foam samples, according to the information provided by the foam manufacturer. However, since the estimation of ϕ_m is characterized by substantial uncertainty, its value is considered to be in the range from 0.05 to 0.25 for the present investigation, based on the typical information gathered from different foam producers as well as the in-house experience acquired over the past several years [32]. In order to cover the expected range, three different values of ϕ_m are considered for the binarization of 3D CT-scan data of the foam samples, namely 0.05, 0.15 and 0.25.

Fig. 6 presents the predictions of ETC due to pure heat conduction $k_{eff,C}$ in different directions as functions of the average temperature, for different microscopic porosities. It can be easily observed from the figure that $k_{eff,C}$ varies for the different directions, which indicates the presence of anisotropy within the foam samples. This observation is clearly in agreement with the corresponding structural analysis (refer to the values of $\overline{D}_{x,y,z}$ in Table 1) and it can be safely concluded that $k_{eff,C}$ is higher in the x-direction, where the pores are distinctly elongated [32]. Moreover, irrespective of the direction, $k_{eff,C}$ clearly decreases with the increase in the average operating temperature in a manner similar to that observed for k_B, although the converse occurs for k_f (see Eq. (12) for clarification). This may be explained by the fact that since $k_B/k_f \gg 1$ for the investigated range of temperature, the contribution of the thermal conductivity k_B of the bulk solid material to $k_{eff,C}$ dominates over that of the fluid. It may also be observed from Fig. 6 that irrespective of the direction, $k_{eff,C}$ increases with ϕ_m, although the opposite occurs for k_s according to Eq. (11), as previously reported by Goetze et al. [32] and presented in Fig. 5(c). However, this effect becomes less pronounced at higher temperatures. In the direction of elongated pores, i.e. in the x-direction, the effect of ϕ_m on $k_{eff,C}$ is minimal, as may be observed from Fig. 6.

The extinction coefficient β is evaluated for different ϕ_m using the image superposition technique [27,29,30], as described in Section 3.2. The image superposition technique is valid even in presence of microscopic porosity since these micropores are present only inside the struts that appear optically solid from outside, i.e. when viewed through the macropores capture by the CT-scan imaging. However, since the dimensions of the present samples are quite large (60 mm × 120 mm × 120 mm), they are decomposed into sub-samples of smaller dimensions (20 mm × 20 mm × 20 mm). While evaluating β for each sub-sample in different directions, results for foam thicknesses L smaller than the directional mean pore diameter $\overline{D}_{x,y,z}$ are eliminated from the evaluation. The minimum, the average and the maximum values of β (i.e. β_{min}, β_{av} and β_{max}, respectively) are then calculated based on the data for the remaining part of the sub-sample, as explained in Fig. 7(a). However, it was pointed out by Mendes et al. [29,30] that β_{max} may be considered as a better estimation for the true value of β as compared to β_{av} or β_{min} and hence $\beta = \beta_{max}$ is adopted for the subsequent calculations. This assumption is also in agreement with that reported by Loretz et al. [27], where the extinction coefficient, estimated from the image superposition technique, was compared with the respective measurements for metal foams. Following this procedure, the extinction coefficient β of the foam is calculated in different directions as the average value of all individual sub-samples (see Fig. 7) and the results are presented in Table 2 for different values of ϕ_m.

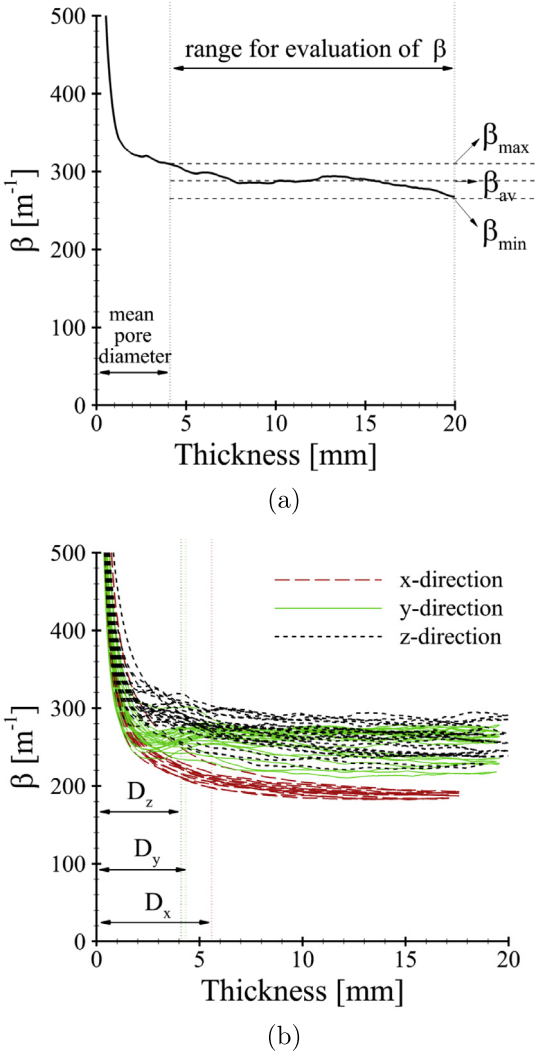

Fig. 7. Extinction coefficient β as function of foam thickness L for sub-samples of smaller dimensions (20 mm × 20 mm × 20 mm) with $\phi_m = 0.15$: (a) methodology for evaluating the minimum, average and maximum values of β; (b) variations of β for all sub-samples in different directions.

It may be observed from Fig. 7(b) that the directional values of β present large variations among different sub-samples, where this variation is comparatively small in the direction of the elongated pores. Considering the variations in $\overline{D}_{x,y,z}$ shown in Table 1, which quantify the pore elongation, it may also be concluded from Fig. 7 (b) as well as Table 2 that (as expected), for a fixed value of ϕ_m, β decreases with the increase in directional mean pore diameter. In addition, Table 2 also shows that the directional value of β increases with ϕ_m, since higher values of ϕ_m yield lower values of ϕ_M according to Eq. (10), as shown in Fig. 5(a). Consequently, a higher fraction of the modeled solid phase, that also includes microscopic porosity and is idealized to be opaque, obstructs the propagation of radiation through the fluid phase (to a greater extent) and eventually increases the directional extinction coefficient (see Fig. 5(b)).

The predictions of directional ETC due to coupled conduction and radiation, obtained employing $k_{eff,C}$ and β as reported in Fig. 6 and Table 2, respectively, are presented as functions of the average temperature in Fig. 8 for different values of ϕ_m. Comparing Figs. 6 and 8, it may be readily observed that for lower average temperatures, k_{eff} increases with the increase in ϕ_m in a manner similar to that observed for $k_{eff,C}$, since the radiation heat transfer has only a marginal influence on ETC. However, as the average temperature increases, the contribution of radiative energy transport to k_{eff} becomes important and hence ETC decreases with the increase in ϕ_m due to the consequent increase in β, as shown in Table 2. Consequently, there is an intermediate range of the average temperature, as shown in Fig. 8, where the opposite influence of ϕ_m on the conductive ($k_{eff,C}$) and radiative heat transfer compensate each other and hence k_{eff} is less sensitive to the variation in ϕ_m. Nevertheless, it is also evident from Fig. 8 that this intermediate temperature range is direction-dependent owing to the structural anisotropy of the foam.

Another expected observation from Fig. 8 is that irrespective of the direction and ϕ_m, with the initial increase in the average temperature, k_{eff} first decreases owing primarily to the decrease in $k_{eff,C}$ since radiation heat transfer is insignificant for the lower range of operating temperature. On the contrary, at higher average temperatures, k_{eff} increases rapidly since the contribution of radiation dominates over that of conduction. Quite obviously, an intermediate range of average temperature can be observed from Fig. 8, where k_{eff} is less sensitive to T_{av}.

Fig. 9 presents the comparison between the predicted and the measured values of k_{eff} as functions of the average temperature. In Fig. 9(a), the measurements of k_{eff} for different average temperatures are shown along with the estimated experimental uncertainty. For the simplified 1D homogeneous model, the directional ETCs are presented in the same figure considering both conduction and radiation as well as only conduction, assuming $\phi_m = 0.15$. Taking into account the fact that the considered 10 ppi foams exhibit relatively large pores, it can be clearly concluded from Fig. 9(b) that for temperatures above 200 °C, the consideration of radiation is

Table 2
Extinction coefficients in different directions and macroscopic porosity as functions of microscopic porosity (x, y and z directions are shown in Figs. 1(a) and 2).

ϕ_m	ϕ_M	$\beta = \beta_{max}$ [m^{-1}]		
		x	y	z
0.05	0.884	184	267	273
0.15	0.871	197	288	298
0.25	0.853	211	309	326

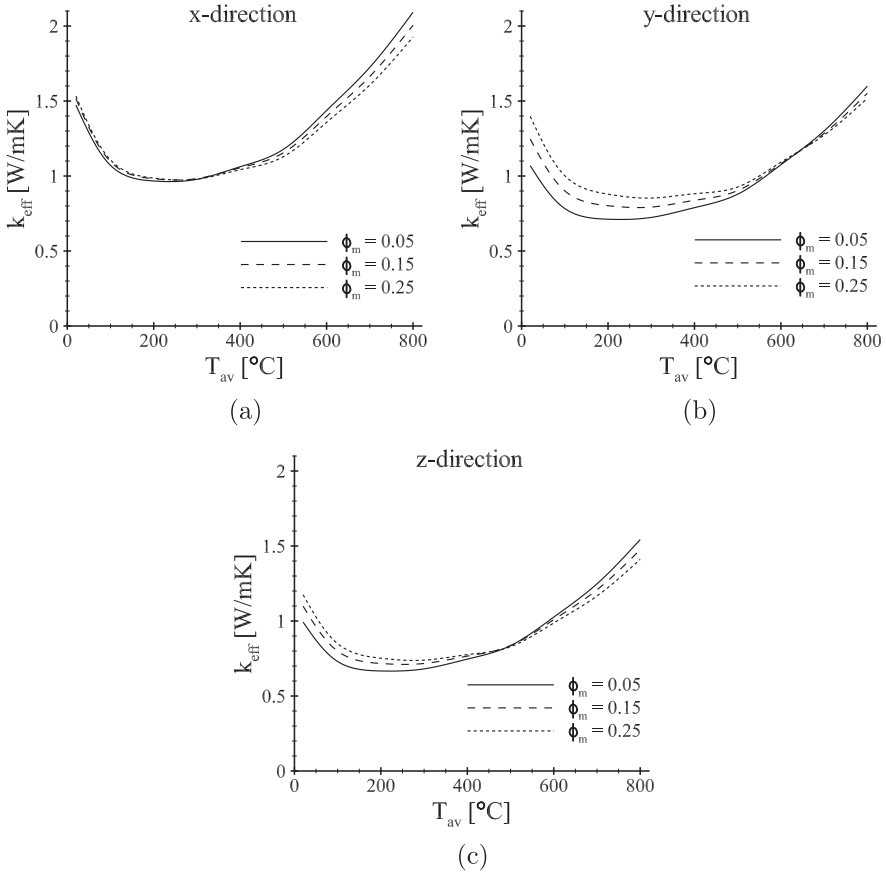

Fig. 8. Predicted directional ETC due to coupled conduction and radiation as function of average temperature for different ϕ_m: (a) x-direction; (b) y-direction; (c) z-direction.

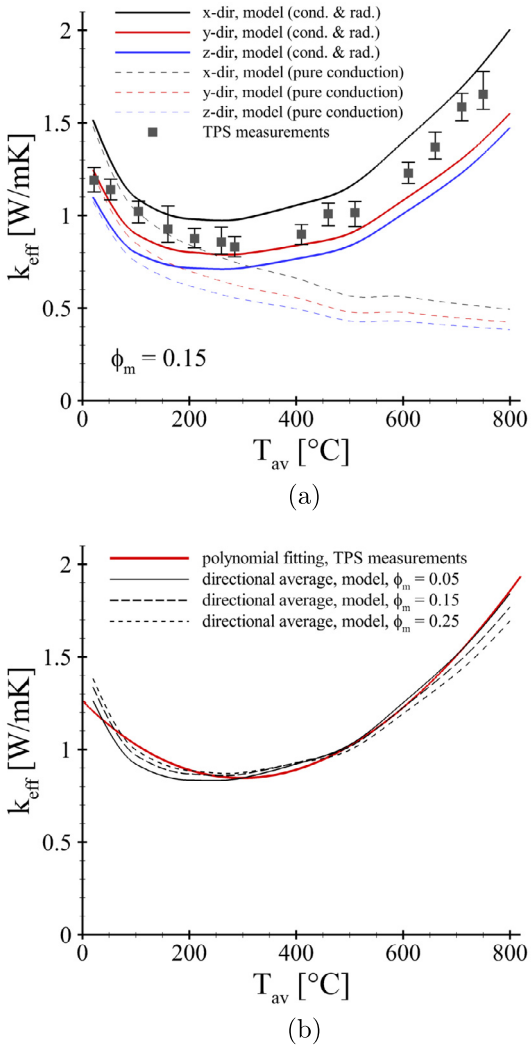

Fig. 9. Comparison between measurements and predictions of ETC as function of the average temperature: (a) raw experimental data and predicted directional ETC; (b) least squares fit of experimental data and weighted directional average prediction for different ϕ_m.

extremely important for an accurate prediction of ETC. In addition, it can be also observed that the experimental data for ETC are mostly bounded by the directional ETC values predicted by the simplified 1D conduction–radiation model. This observation possibly suggests that the TPS technique employed for the present investigation displays a weighted average ETC of the directional values with respect to the desired direction.

In order to allow for a better comparison between the measurements and the predictions, the experimental results for ETC are further post-processed in the following manner. A least squares polynomial fit that represents all experimental data is obtained by assuming a third order polynomial in the average temperature (T_{av}). Additionally, the directional ETC predicted by the model is empirically averaged for the x-direction as:

$$k_{av,x} = \frac{1}{2}\left[k_x + \frac{k_y + k_z}{2}\right] \tag{14}$$

where $k_{av,x}$ is the weighted directional average ETC that is considered based on the following argument. Since the disk shaped planar heat source of TPS apparatus is placed perpendicular to the x-direction and parallel to both y- and z-directions, as shown in Fig. 2, $k_{av,x}$ is obtained as an average of ETC values in these perpendicular and parallel directions, where ETC in the parallel direction itself is taken as an average of ETC in both y- and z-directions. Although Eq. (14) may be regarded as an empirical relation that is not rigorously derived from any theoretical consideration, it may be easily verified that the adopted relation respects at least the limit of isotropic material, i.e. for $k_x = k_y = k_z$, where such averaging would not be required.

Fig. 9(b) shows the least squares polynomial fit of the measured ETC as a function of the average temperature, along with the corresponding conduction–radiation predictions that are post-processed according to Eq. (14). The predictions of ETC are presented for different microscopic porosities in order to provide a rough quantitative idea about the parametric uncertainty associated with the model. Taking this as well as the experimental uncertainty into account, it may be clearly observed that the present predictions are in very good agreement with the experimental data for the complete range of investigated temperature. This supports the argument that TPS technique measures a directionally averaged ETC, according to Eq. (14). After appropriate validation, which would require several case studies involving porous foams of different materials, pore densities and sizes, this approach could provide a viable experimental procedure based on TPS technique that would allow the measurement of true directional ETC of anisotropic foams. ETC could be measured in all three directions by orienting the foam surfaces perpendicular to the respective direction and then applying a weighted average formula, similar to Eq. (14), in order to recover the true ETC in these directions. However, this extended study is kept beyond the scope of the present investigation and in all probability, would be taken up in near future.

5. Conclusions

In the present study, TPS technique is used in order to measure ETC of 10 ppi open-cell ceramic foams made of pure alumina. The detailed morphology of the foam structures is reconstructed from 3D CT-scan images. The structural analysis of the foam samples is carried out using a volume image processing tool. The experimental results are compared with the predictions of directional ETC obtained using the simplified 1D homogeneous model, proposed and validated earlier by Mendes et al. [29,30]. The effective thermal conductivity due to pure heat conduction and the extinction coefficient, required by the model, are evaluated based on the 3D CT-scan data.

From the present investigation, the following major conclusions can be drawn:

1. The predictions of ETC for the ceramic foams can be clearly correlated with the geometric parameters obtained from their structural analysis. In this respect, the degree of foam anisotropy, indicated by the pore dimensions in different directions, plays an important role and the predicted ETC is observed to be higher in the directions in which the pores are more elongated.
2. The estimated microscopic porosity (ϕ_m) of the foams, which cannot be captured by 3D CT-scan images, has considerable influence on the reconstructed foam structure and hence on the predictions of ETC. The conduction and radiation modes of heat transfer depend on ϕ_m in an opposite manner and hence the overall ETC is strongly dictated by the dominant heat transfer mode, which in turn depends on the foam temperature.
3. The measurements of ETC, obtained with TPS technique, can be interpreted as a directionally averaged value of ETC in three perpendicular directions (see Eq. (14)). The predictions of directional ETC, obtained after the proposed averaging, correspond very well with TPS measurements in the investigated range of temperatures. Nevertheless, additional investigations are rec-

ommended in order to further clarify this issue and exploit the observations for developing a measurement technique that can determine the true directional ETC of anisotropic open-cell porous foams.

Acknowledgments

The authors gratefully thank the German Research Foundation (DFG) for supporting the investigation in subprojects B02 and B03, that are part of the Collaborative Research Center CRC 920.

References

[1] M. Mendes, J. Pereira, J. Pereira, On the stability of ultra-lean H2/CO combustion in inert porous burners, Int. J. Hydrogen Energy 33 (2008) 3416–3425.
[2] S. Gauthier, A. Nicolle, D. Baillis, Investigation of the flame structure and nitrogen oxides formation in lean porous premixed combustion of natural gas/hydrogen blends, Int. J. Hydrogen Energy 33 (2008) 4893–4905.
[3] S. Voss, M. Mendes, J. Pereira, S. Ray, J. Pereira, D. Trimis, Investigation on the thermal flame thickness for lean premixed combustion of low calorific H2/CO mixtures within porous inert media, Proc. Combust. Inst. 34 (2013) 3335–3342.
[4] F.C. Patcas, G.I. Garrido, B. Kraushaar-Czarnetzki, CO oxidation over structured carriers: a comparison of ceramic foams, honeycombs and beads, Chem. Eng. Sci. 62 (2007) 3984–3990.
[5] A. Sommers, Q. Wang, X. Han, C. T'Joen, Y. Park, A. Jacobi, Ceramics and ceramic matrix composites for heat exchangers in advanced thermal systems - A review, Appl. Therm. Eng. 30 (2010) 1277–1291.
[6] O. Dávila-Maldonado, A. Adams, L. Oliveira, B. Alquist, R.D. Morales, Simulation of fluid and inclusions dynamics during filtration operations of ductile iron melts using foam filters, Metall. Mater. Trans. B 39 (6) (2008) 818–839.
[7] M.L. Becker, S. Decker, F.J. Durst, D. Trimis, S.D.J. Nemoda, V. Stamatov, M. Steven, Thermisch beaufschlagte Porenkörper und deren Durchströmungs- und Wärmeübertragungs-eigenschaften, DFG Projekt DU 101/55-1, Abschlussbericht, Deutsches Zentrum für Luft- und Raumfahrt, 2002.
[8] G.-Q. Wang, S.-J. Huang, N. Ding, D. Luo, X.-F. Huang, Y. Liu, J.-R. Xu, Characteristics of the effective thermal conductivity of highly porous ceramic foam, Proc. CSEE 30 (10) (2010) 73–78.
[9] B. Dietrich, G. Schell, E.C. Bucharsky, R. Oberacker, M.J. Hoffmann, W. Schabel, M. Kind, H. Martin, Determination of the thermal properties of ceramic sponges, Int. J. Heat Mass Transfer 53 (2010) 198–205.
[10] B. Dietrich, T. Fischedick, M. Wallenstein, M. Kind, Thermal conductivity of ceramic sponges at temperatures up to 1000 °C, Special Topics Rev. Porous Media 6 (2015) 133–143.
[11] T. Fischedick, M. Kind, B. Dietrich, High temperature two-phase thermal conductivity of ceramic sponges with stagnant fluid experimental results and correlation including thermal radiation, Int. J. Therm. Sci. 96 (2015) 1–11.
[12] D.-W. Liaw, C.-Y. Tsai, W.-C.J. Wei, Thermal insulation of muscovite/glass ceramic foam for solid oxide fuel cell, J. Power Sources 196 (2011) 8012–8018.
[13] B.S. Skidan, S.A. Borisov, A study of effective thermal conduction in lightweight foam corundum refractories, Refract. Ind. Ceram. 44 (2003) 355–356.
[14] Y.W. Lo, W.C.J. Wei, C. Hsueh, Low thermal conductivity of porous Al_2O_3 foams for SOFC insulation, Mater. Chem. Phys. 129 (2011) 326–330.
[15] R. Coquard, D. Rochais, D. Doermann-Baillis, Experimental investigatons of the coupled conductive and radiative heat transfer in metallic/ceramic foams, Int. J. Heat Mass Transfer 52 (2009) 4907–4918.
[16] J. Sacadura, D. Baillis, Experimental characterization of thermal radiation properties of dispersed media, Int. J. Therm. Sci. 41 (2002) 699–707.
[17] R. Coquard, D. Baillis, Radiative and conductive thermal properties of foams, in: A. Öchsner, G. Murch, M.D. Lemos (Eds.), Cellular and Porous Materials: Thermal Properties Simulation and Prediction, John Wiley & Sons, 2008, pp. 343–384.
[18] R. Coquard, D. Rochais, D. Baillis, Conductive and radiative heat transfer in ceramic and metal foams at fire temperatures, Fire Technol. 48 (2012) 699–732.
[19] A. Druma, M. Alam, C. Druma, Analysis of thermal conduction in carbon foams, Int. J. Therm. Sci. 43 (2004) 689–695.
[20] P. Talukdar, M. Mendes, R. Parida, D. Trimis, S. Ray, Modelling of conduction–radiation in a porous medium with blocked-off region approach, Int. J. Therm. Sci. 72 (2013) 102–114.
[21] M.A. Mendes, S. Ray, D. Trimis, A simple and efficient method for the evaluation of effective thermal conductivity of open-cell foam-like structures, Int. J. Heat Mass Transfer 66 (2013) 412–422.
[22] J. Storm, M. Abendroth, M. Emmel, T. Liedke, U. Ballaschk, C. Voigt, T. Sieber, M. Kuna, Geometrical modelling of foam structures using implicit functions, Int. J. Solids Struct. 50 (2013) 548–555.
[23] S. Cunsolo, R. Coquard, D. Baillis, N. Bianco, Radiative properties modeling of open cell solid foam: review and new analytical law, Int. J. Therm. Sci. 104 (2016) 122–134.
[24] J. Petrasch, P. Wyss, A. Steinfeld, B. Schrader, Tomography-based determination of the effective thermal conductivity of fluid-saturated reticulate porous ceramics, ASME J. Heat Transfer 130 (2008) 032602.
[25] R. Coquard, D. Baillis, Numerical investigation of conductive heat transfer in high-porosity foams, Acta Mater. 57 (2009) 5466–5479.
[26] J. Petrasch, P. Wyss, A. Steinfeld, Tomography-based Monte Carlo determination of radiative properties of reticulate porous ceramics, J. Quant. Spectrosc. Radiat. Transfer 105 (2007) 180–197.
[27] M. Loretz, E. Maire, D. Baillis, Analytical modelling of the radiative properties of metallic foams: contribution of X-ray tomography, Adv. Eng. Mater. 10 (2008) 352–360.
[28] P. Parthasarathy, P. Habisreuther, N. Zarzalis, Identification of radiative properties of reticulated ceramic porous inert media using ray tracing technique, J. Quant. Spectrosc. Radiat. Transfer 113 (2012) 1961–1969.
[29] M.A. Mendes, P. Talukdar, S. Ray, D. Trimis, Detailed and simplified models for evaluation of effective thermal conductivity of open-cell porous foams at high temperatures in presence of thermal radiation, Int. J. Heat Mass Transfer 68 (2014) 612–624.
[30] M.A. Mendes, V. Skibina, P. Talukdar, R. Wulf, U. Gross, D. Trimis, S. Ray, Experimental validation of simplified conduction–radiation models for evaluation of effective thermal conductivity of open-cell metal foams at high temperatures, Int. J. Heat Mass Transfer 78 (2014) 112–120.
[31] R.G. Munro, Evaluated material properties for a sintered α-alumina, J. Am. Ceram. Soc. 80 (1997) 1919–1928.
[32] P. Goetze, M.A. Mendes, A. Asad, H. Jorschick, E. Werzner, R. Wulf, D. Trimis, U. Gross, S. Ray, Sensitivity analysis of effective thermal conductivity of open-cell ceramic foams using a simplified model based on detailed structure, Spec. Top. Rev. Porous Media: An Int. J. 6 (2015) 1–10.
[33] S.E. Gustafsson, Transient plane source techniques for thermal conductivity and thermal diffusivity measurements of solid materials, Rev. Sci. Instrum. 62 (1991) 797–804.
[34] R. Wulf, M.A. Mendes, V. Skibina, A. Al-Zoubi, D. Trimis, S. Ray, U. Gross, Experimental and numerical determination of effective thermal conductivity of open cell FeCrAl-alloy metal foams, Int. J. Therm. Sci. 86 (2014) 95–103.
[35] R. Coquard, E. Coment, G. Flasquin, D. Baillis, Analysis of the hot-disk technique applied to low-density insulating materials, Int. J. Therm. Sci. 65 (2013) 242–253.
[36] V. Bohac, M.K. Gustavsson, L. Kubicar, S.E. Gustafsson, Parameter estimations for measurements of thermal transport properties with the hot disk thermal constants analyzer, Am. Inst. Phys. 71 (2000) 2252–2255.
[37] S. Patankar, Numerical Heat Transfer and Fluid Flow, Hemisphere Publishing Corporation, New York, 1980.
[38] M. Modest, Radiative Heat Transfer, second ed., Academic Press, New York, 2003.
[39] N. Shah, New method of computation of radiation heat transfer in combustion chambers, Imperial College, University of London, England, 1979. Ph.D. thesis.
[40] P. Coelho, M. Carvalho, A conservative formulation of the discrete transfer method, ASME J. Heat Transfer 119 (1997) 118–128.
[41] P. Talukdar, Discrete transfer method with the concept of blocked-off region for irregular geometries, J. Quant. Spectrosc. Radiat. Transfer 98 (2006) 238–248.
[42] S.C. Mishra, P. Talukdar, D. Trimis, F. Durst, Computational efficiency improvements of the radiative transfer problems with or without conduction – a comparison of the collapsed dimension method and the discrete transfer method, Int. J. Heat Mass Transfer 46 (2003) 3083–3095.
[43] Z. Hashin, S. Shtrikman, A variational approach to the theory of the effective magnetic permeability of multiphase materials, J. Appl. Phys. 33 (1962) 3125–3131.
[44] O. Rozenbaum, D.D.S. Meneses, Y. Auger, S. Chermanne, P. Echegut, A spectroscopic method to measure the spectral emissivity of semi-transparent materials up to high temperature, Rev. Sci. Instrum. 70 (1999) 4020–4025.
[45] F. Incropera, D. DeWitt, T. Bergman, A. Lavine, Fundamentals of Heat and Mass Transfer, sixth ed., John Wiley & Sons, Hoboken, 2007.
[46] VDI-Gesellschaft Verfahrenstechnik und Chemieingenieurwesen, VDI Heat Atlas, second ed., Springer, Berlin, 2010.